Figure 10

Observed temperatures at the Firth of Thames mooring for May 2003

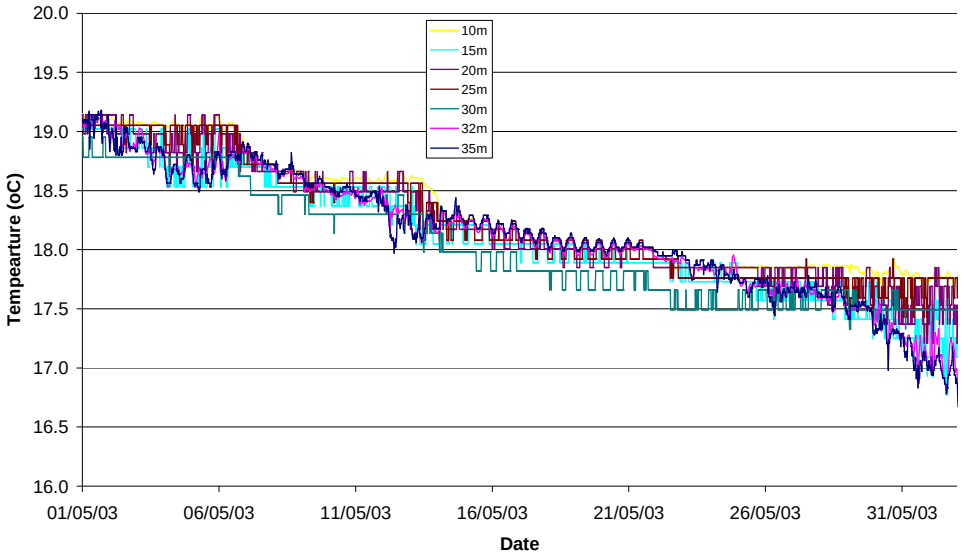

3.3.4 Salinity

Figure 11

Observed salinities at the Firth of Thames mooring for May 2003. The two lines correspond to temperatures measured at 10 m and 22 m above the sea-bed.

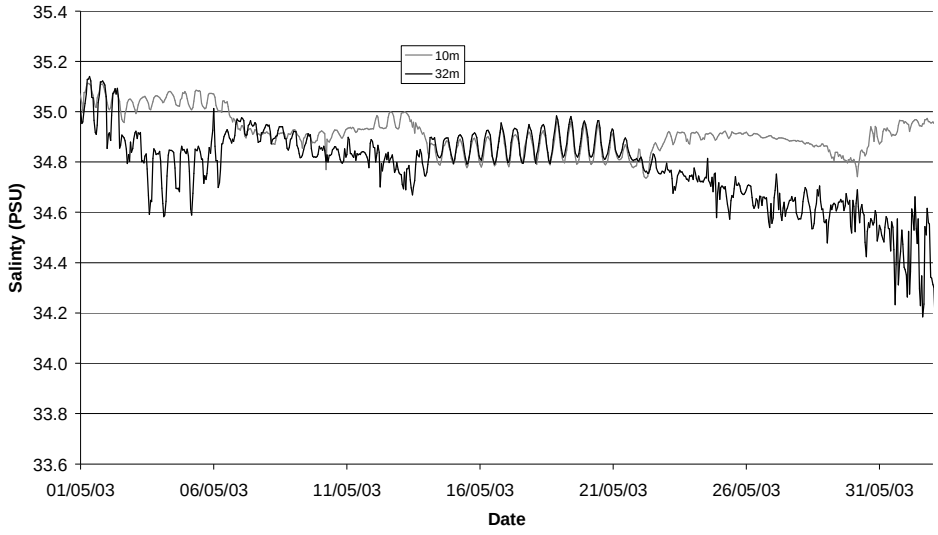

The observed salinity variations at the Firth of Thames mooring site (Figure 11) were applied to the open boundary. Surface salinity was set to the observed salinity at 32m above the sea-bed. Salinity at cells closer than 10m to the bed ware set to the observed values at 10m above the bed. Values in between were linearly interpolated.

The background salinity was set to 35.3 psu. River salinities were set to 4 psu.

3.3.5 Wind

To force the calibrated model simulations, wind data were obtained from weather stations at Auckland, Leigh, Mokohinau Islands, Onehunga, Paeroa, Whangaparoa and Whangarei. Duplicate data were removed and gaps were filled using linear interpolation (largest gap was 6 hrs). Data from the seven stations were interpolated over the Hauraki Gulf grid area using a cubed inverse-distance routine and the file then cropped to the Firth of Thames model region. The default wind friction coefficient was used for the simulations. Figure 12 shows the wind data from the Mokohinau A wind station.

Figure 12

(A) Wind speed and (B) direction from the Mokohinau AWS for May 2003. Data is plotted in meteorological convention (direction from which the wind blows).

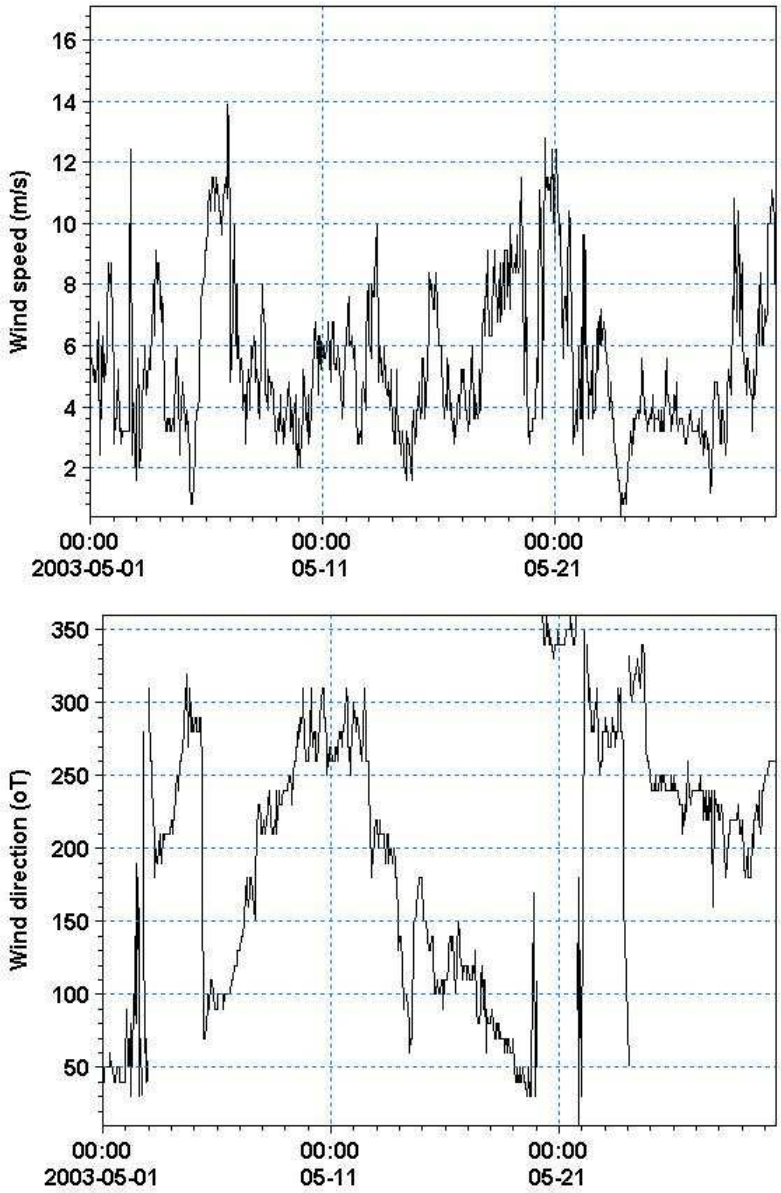

3.3.6 Heat exchange

Dry-bulb temperature readings from Auckland, Leigh, Mokohinau Islands and Paeroa were averaged to create a temperature timeseries for input to the model (Figure 13).

Figure 13
Air temperature time series used for model simulations.

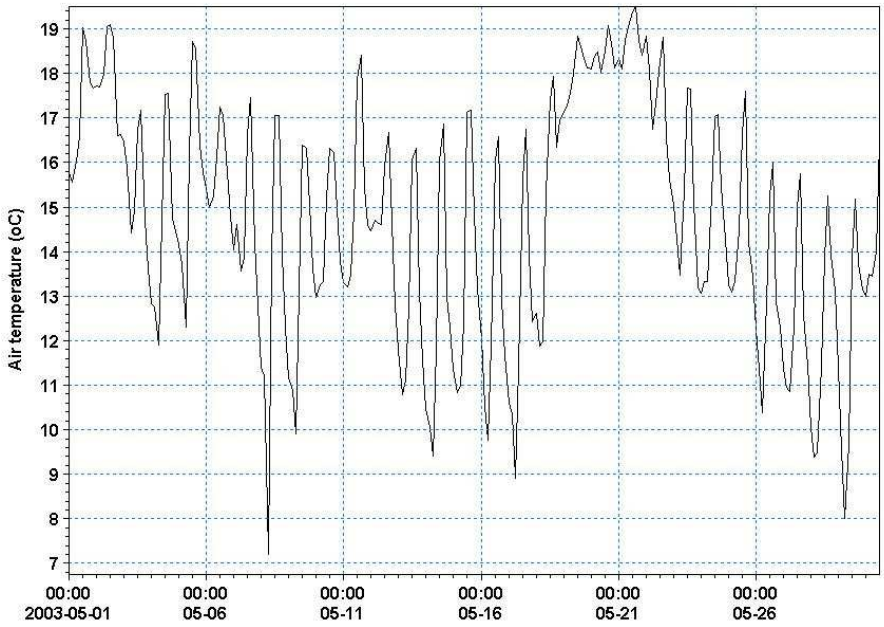

3.3.7 Relative Humidity

Humidity is an important control on air-sea heat exchange. In the absence of sea-based measurements, relative humidity measurements from land-based weather stations were trialled, but these did not provide any better results than the default value of 88%, so relative humidity was set to 88% in the model.

3.4 Model output

Velocity in the horizontal and vertical directions, temperature and salinity were output at ½-hour intervals.

Whilst it is conceivable that large-scale farm development may modify flow patterns, this has not been accounted for in our simulations. Initial studies have shown that currents do slow as they pass through marine farms, but the extent of retardation is not well known. Enhanced friction and slower flows will affect the amount of time that material is held inside the farm domain, and may therefore effect biomass estimates *inside* the farm area. The presence of farms is unlikely to greatly modify hydrodynamics in the Firth of Thames, and therefore should have only minor affect on transport in the far-field outside the farms.

4 Methods (Biological models)

Within this section we aim to describe how: a) the Area A farms were represented within the plankton models; (b) the sampling protocols of the synoptic survey were approximated within the models and (c) summarise other relevant details regarding the simulations.

4.1 Implementing the farming system

Our models do not explicitly represent either the individual dropper lines, or the individual 2.75 ha farm blocks. Instead, we represent Area A as three sub-areas (Figure 1). The total number of mussels (of each size-class) within a sub-area was derived from the total surface area of the sub-area (less area devoted to inter-block spacing and unstocked blocks), backbones ha^{-1} of stocked block, dropper length $backbone^{-1}$ and mussel density m^{-1} of dropper. This mussel population was implicitly assumed to be evenly dispersed through the entire sub-area (from the sea-surface to the maximum dropper depth).

The same approach was also used to represent the nine small areas of mussel farm off Waimangu point on the western side of the firth – however, we do not discuss these farms further.

4.2 Biological simulations

We made two simulations with the biophysical model and two with the empirical model. In each case, one simulation was a 'no farms' simulation (*ie* no farms present within the domain), and one simulation was a 'with farms' simulation (*ie* the nine small Waimangu point farms and the three sub-areas of Wilson Bay Area A were occupied by farms). In all cases, the simulation period was: 13-30 May 2003.

Inferences concerning the magnitude of (simulated) farm influence are drawn in two ways: (a) direct comparison of the no-farms and with-farms simulation results, and (b) application of the surfaces-method to the simulation results.

The initial conditions for the biophysical model were chosen to be similar to the conditions measured around Wilson Bay on May 13th in the Group A fortnightly monitoring program. We assumed that concentrations of nutrient and organic detritus were spatially homogenous throughout the firth. A similar assumption was made for each of the three phytoplankton taxa.

The initial conditions adopted for the empirical model were identical to those adopted in the earlier work. Specifically, we assumed that the local concentration of each sub-class was equal to the prescribed local carrying capacity (see Broekhuizen et al. 2004).

4.3 Implementing the synoptic survey sampling protocol

As noted in section 2.4, the synoptic survey comprised two components: (a) repeat samples at 49 fixed stations and (b) underway monitoring of water-column characteristics (incl. an indicator of chlorophyll abundance) along fixed transects during the intervening period. We have chosen to focus upon the former data-set.

We have chosen to focus our verification effort upon the station-data. To permit this, we endeavoured to reproduce the station-sampling protocol within the models.

4.3.1 Fixed station sampling & analysis of virtual data

To reproduce the fixed station protocol within the models we first determined in which 750 x 750 m water-column of the model domain each station belonged. Our initial intent was then to record the depth average (sea-surface to lesser of 10 m, or sea-floor depth) concentrations of nutrient and taxon-specific plankton abundance within the appropriate 750 x 750 grid-cell at the appropriate instant in (simulated) time. In practise, model 'sampling error' (see 7.2) proved to be a significant problem when using these instantaneous measures. In an effort to reduce this a little, we therefore calculated station-specific time-and-depth averages over a two hour period (one hour either side of the true sampling time). The models' horizontal and bathymetric resolution are such that several of the inshore-most stations appear to be over dry-land (Figure 2). In these cases, we moved the (model) sampling location into the nearest cell having a water-depth of 5 m or greater.

Our models measure abundance in terms of carbon. Whilst we do have field estimates of phytoplankton carbon abundance at a sub-set of the 5 occasions x 49 fixed stations, we prefer to make the comparison of model results against the chlorophyll data – of which we have far more. For the biophysical model, we converted carbon biomasses to chlorophyll using C:chlorophyll (by weight) ratios of 50:1 (diatoms and phytoflagellates) and 100:1 (dinoflagellates). We adopted a C:chl ratio of 50:1 when comparing the results from the logistic model (which lacks taxonomic resolution).

5 Results (Hydrodynamic model)

Within this section we summarise the calibration of the hydrodynamic model as per the set-up used in Stephens & Broekhuizen (2003).

5.1 Tides

In this section the predicted tide level at the farm site is compared to the observed water level for the period of the synoptic survey (Figure 14). Predicted tides are reproduced well. 54% of the predicted values fall within 0.05 m of the observed data. The slope of the regression between the model and field data is 0.948. The intercept is 0.089 and the regression has an r^2 value of 0.991.

Figure 14
Frequency distribution of the differences between simulated and observed tide height.

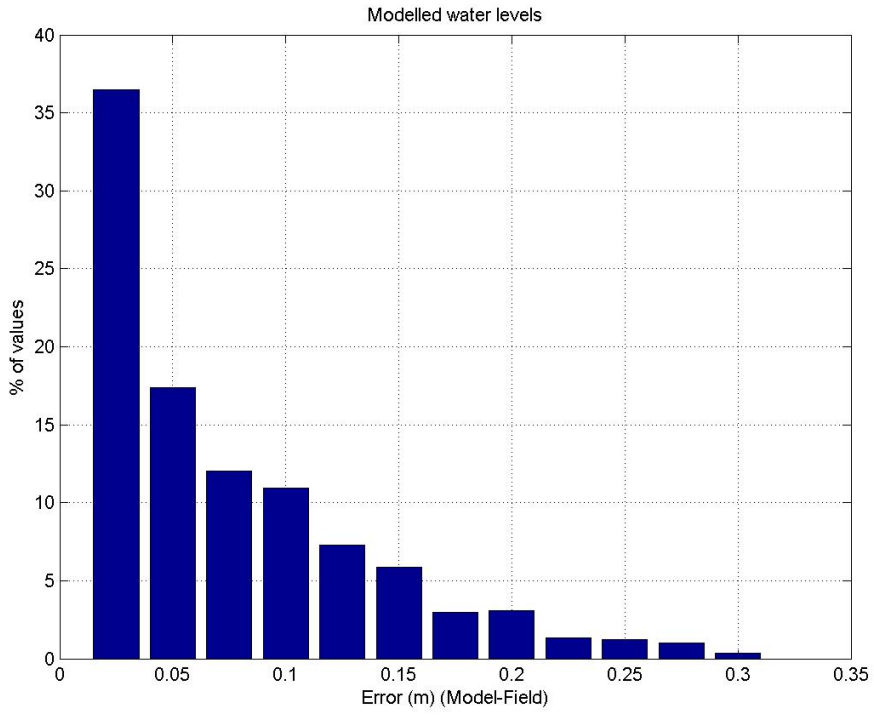

5.2 Currents

In this section the depth-average currents from the Acoustic Doppler Current Profilers (i.e., the average of the bottom, mid and top ADPC record) are compared to the predicted depth-averaged currents from the model (i.e., the average value from all the layers within the model at the cell corresponding to the ADCP site (Figure 15).

Figure 15

Frequency distribution of the difference between simulated and observed current speeds in (a) EW direction at site D, (b) NS directions at site D, (c) EW direction at site C, (d) NS direction at site C.

a

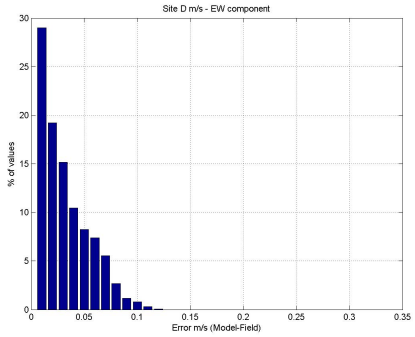

b

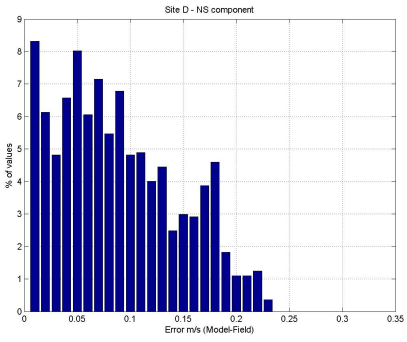

c

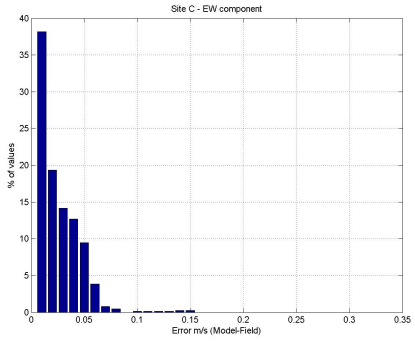

d

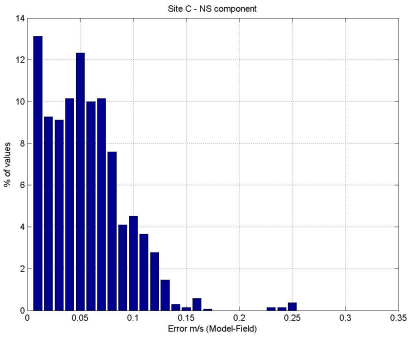

Predicted currents at Site D are reproduced well. 82% of the predicted east-west velocity component falls within 0.05 m/s of the observed data. The slope of the regression between the modelled east-west velocity and field data is 0.728. The intercept is 0.038 and the regression has an r^2 value of 0.734.

34% of the predicted north-south velocity component falls within 0.05 m/s of the observed data. The slope of the regression between the modelled east-west velocity and field data is 0.525. The intercept is 0.048 and the regression has an r^2 value of 0.506.

Predicted currents at Site C are well modelled. 94% of the predicted east-west velocity component falls within 0.05 m/s of the observed data. The slope of the

regression between the modelled east-west velocity and field data is 0.306. The intercept is -0.070 and the regression has an r^2 value of 0.462.

54% of the predicted north-south velocity component falls within 0.05 m/s of the observed data. The slope of the regression between the modelled east-west velocity and field data is 0.429. The intercept is 0.062 and the regression has an r^2 value of 0.503.

5.3 Stratification (Salinity & Temperature)

In this section the predicted salinity and temperature variation with depth for each day of the synoptic survey is presented for Transect A. The solid line in the plots indicates the average salinity values for the day of the survey for the sites that fall within the corresponding model cell (Figure 16). The symbols in the plots show the range of salinities that the model predicts over the tidal cycle that spans the time of the synoptic survey. It can be seen that the model predicts the stratification present at the start of the synoptic survey (25th, Figure 16a) and also tracks the increase in salinity and temperature observed over the last days of the synoptic survey (28th-29th, Figure 16c,d). Data from other transects reveal similarly good fits between the modelled and observed stratification.